O-doped nanographenes: the pyrano/pyrylium route towards semiconducting cationic mixed valence complexes

Luka Đorđević, Cataldo Valentini, Nicola Demitri, Cécile Mézière, Magali Allain, Marc Sallé, Andrea Folli, Damien Murphy, Samuel Mañas-Valero, Eugenio Coronado and Davide Bonifazi*

[*] Dr. L. Đorđević, C. Valentini, Dr. A. Folli, Prof. Dr. D. Murphy, Prof. Dr. D. Bonifazi; School of Chemistry, Cardiff University, Main Building, Park Place, Cardiff CF10 3AT, United Kingdom. Email: bonifazid@cardiff.ac.uk

Dr. N. Demitri; Elettra – Sincrotrone Trieste, S.S. 14 Km 163.5 in Area Science Park, 34149 Basovizza, Trieste, Italy

C. Mézière, M. Allain, Prof. Dr. M. Sallé; MOLTECH-Anjou - UMR CNRS 6200, UNIV Angers, SFR Matrix, 2 Boulevard Lavoisier, 49045 Angers Cedex, France

S. Mañas-Valero, Prof. Dr. E. Coronado; Instituto de Ciencia Molecular, Universitat de València, Catedrático José Beltrán 2, 46980 Paterna, Spain

[**] D.B. gratefully acknowledge the EU through the ERC Starting Grant "COLORLANDS", the MC-RISE "INFUSION" and MC-ITN "PHOTOTRAIN" projects and the School of Chemistry at Cardiff University for financial support. The work in Spain has been financed by the MINECO (grants MAT2017-89993-R and Excellence Unit María de Maeztu MDM-2015-0538) and the Generalidad Valenciana (Prometeo Programme). The authors thank Prof. R. Herges (Kiel University) for providing the AICD program, Prof. A. Stanger (Technion Israel

institute of Technology) for sharing the Aroma package and Dr. A. Fermi (Cardiff University) for the spectro-electrochemical measurements.

Supporting information for this article is available on the WWW under http://www.angewandte.org or from the author. Crystallographic data for the structures reported in this paper have been deposited at the Cambridge Crystallographic Data Centre as supplementary publication no. 1557894 (**1_o**), 1920493 (**5**), 1557895 (**2_o**·$^1/_3CH_2Br_2$), 1557896 (**3_oCl_2**·$^1/_5CH_2Br_2$), 1912053 ((**1_o**)$_{10}$(PF_6)$_6$·(THF)$_{16}$) and 1936956 ((**3_o**)$_3$(ClO_4)$_2$·THF·$^1/_2H_2O$).

Abstract: Herein we report an efficient synthesis to prepare O-doped nanographenes, which derive from the longitudinally and latitudinally π-extension of pyrene. The derivatives are highly fluorescent and feature low-oxidation potentials. Exploiting electrooxidation, crystals of cationic mixed valence (MV) complexes were grown in which the organic salts organize into face-to-face π-π stacks, a favorable solid-state arrangement for organic electronics. Variable-temperature EPR measurements and relaxation studies suggest a strong electron delocalization along the longitudinal axis of the columnar π-stacking architectures. Electric measurements of single crystals of the MV salts exhibited a semiconducting behavior with a remarkable high conductivity at room temperature. These findings further support the idea for which the π-extension of polycyclic aromatic hydrocarbons featuring precise heteroatom doping topologies, is an attractive approach to enable nanographenes with a broad spectrum of semiconducting properties and high charge mobilities.

Keywords: polycyclic aromatic hydrocarbons – heteroatom doping – oxonium – pyrylium – pyrano rings – molecular graphenes – EPR – mixed valence complexes – electrocrystallization.

Figure to the table of content

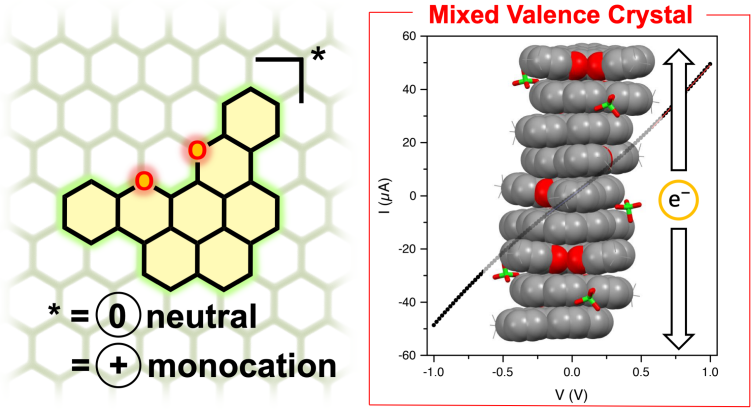

Introduction

The engineering of polycyclic aromatic hydrocarbons (PAHs)[1] has recently enticed great attention for materials exploration as organic semiconductors.[2] Replacing carbon atoms with other isolobal atoms, *i.e.* doping,[3] is emerging as a powerful approach to control the chemical, supramolecular and optoelectronic properties of PAHs. Recent examples include period 2 elements like B-,[4] N-,[5] and O-[6] PAHs. Furthermore, the doping of PAHs allows the synthesis of structures that are difficult to be prepared as full-carbon.[7]

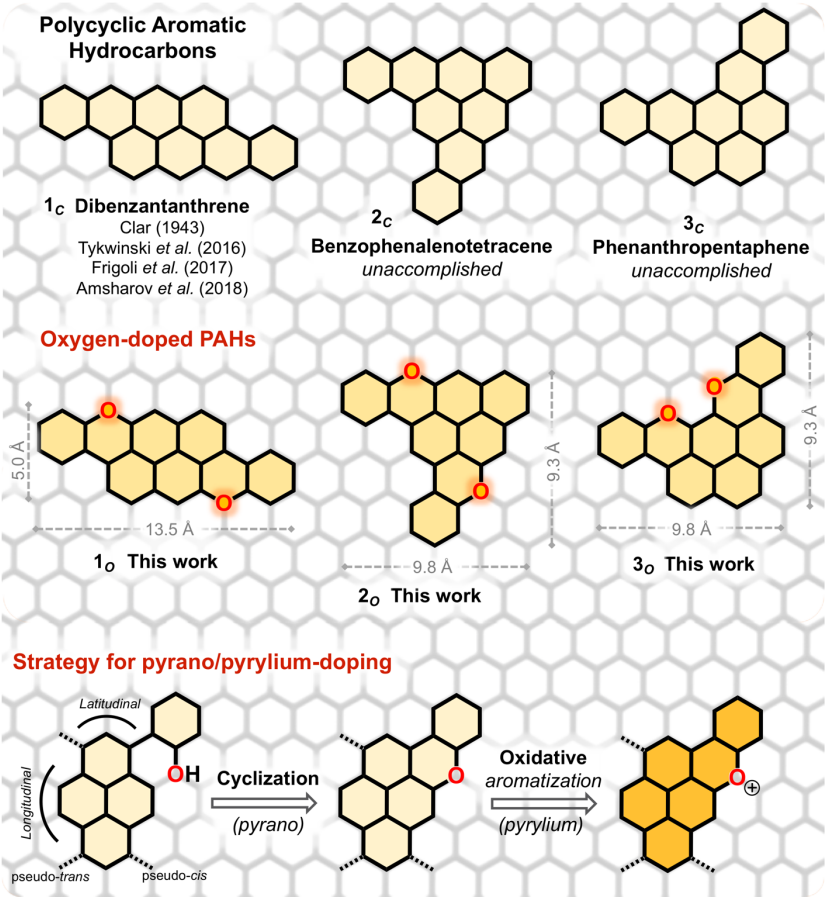

Fig. 1. Structural frameworks of all-carbon (top) and O-doped (center) PAHs discussed in this work, along with the synthetic approach (bottom).

Inspired by the chemical structures of natural anthocyanins[8] and artificial π-expanded xanthenium cations,[9] we inferred that pyranyl and pyrylium rings[10] could be used to prepare O-doped congeners of PAHs **1c–3c** and used to engineer p-type organic semiconductors. Out of the three **1c–3c** PAHs (Fig. 1, top), attention has been placed only on dibenzanthanthrene (**1c**)[11] and its derivatives,[12] finding

applications in single-molecule transistors,[13] optical interaction with alkali atoms for quantum memory,[14] single emitter for super-resolution microscopy[15] and semiconductors with high mobility in solution-processed OFETs.[12b]

Building on this hypothesis, herein we report a robust synthetic approach towards the preparation unprecedented oxygen-containing O-doped PAHs **1o**–**3o** (Fig. 1, middle), in which two carbon atoms have been replaced by two oxygen atoms. At the structural level, this entails the replacement of two fused benzene rings by two pyranyl cycles. The resulting structures reflect disubstituted pyrenes (with a latitudinal or longitudinal substitution pattern, depending on the targeted isomer) with two phenols as key core and peripheral moieties, respectively (Fig. 1, bottom). To favor solubility, all molecules were decorated with *t*-butyl groups (Scheme 1). Capitalizing on the Pummerer oxidative cyclisation[16] of *peri*-xanthenoxanthene (PXX), we expected that this protocol could also lead to isolated pyranyl rings,[17] that in turn could be oxidized into pyrylium cations (Fig. 1, bottom). Interestingly, mixed valence (MV) complexes could be formed at the solid state between the electron-donor pyranyl molecules and its cationic pyrylium derivatives, generating p-type organic semiconductors.

Results and Discussion

We first prepared 1,6-dibromopyrene (**4**) and 1,8-diiodopyrene (**10**) precursors through regioselective bromination (Br_2 in $CHCl_3$) and iodination (I_2 and KIO_3 in $CH_3COOH/H_2O/H_2SO_4$) of pyrene, respectively (Scheme 1).[18] Regarding the 1,3-dibromo isomer (**7**), the pyrenyl core was first mono *tert*-butylated and then dibrominated with NBS. Suzuki-Miyaura cross-coupling reaction between the relevant dihalide pyrenyl precursor and 2-methoxyphenylboronic acid, using $[Pd(PPh_3)_4]$ catalyst, gave access to phenol-bearing pyrenes **6**, **9** and **12** in excellent yields, after demethylation reaction with BBr_3. Final Pummerer oxidative ring-closure with CuO in $PhNO_2$ under reflux conditions yielded O-doped PAHs **1o**–**3o** in very good yields.

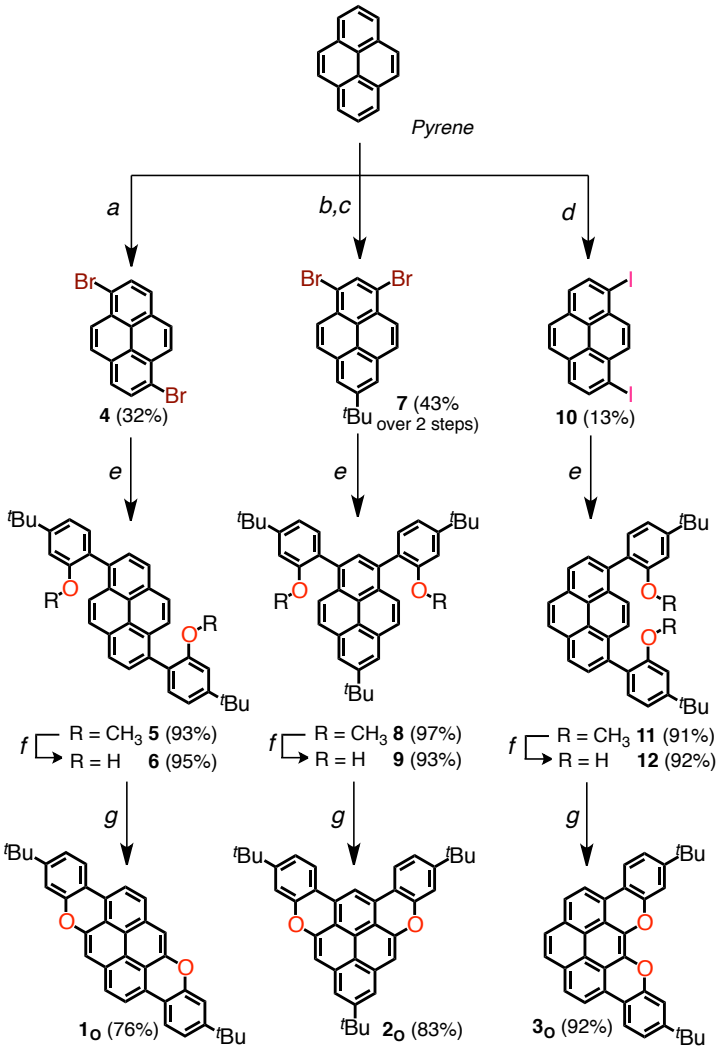

Scheme 1. Synthetic routes to $\mathbf{1_o}$, $\mathbf{2_o}$ and $\mathbf{3_o}$. Reagents and conditions: *(a)* Br_2, $CHCl_3$, r.t.; *(b)* ^{t}BuCl, $AlCl_3$, CH_2Cl_2, r.t.; *(c)* NBS, THF, 30 °C; (*d*) I_2, KIO_3, $CH_3COOH/H_2O/H_2SO_4$, 40 °C; *(e)* (4-(*tert*-butyl)-2-methoxyphenyl)boronic acid, $[Pd(PPh_3)_4]$, NaOH, dioxane/H_2O, reflux; (*f*) BBr_3, CH_2Cl_2, 0 °C → r.t.; *(g)* CuO, $PhNO_2$, reflux.

Suitable crystals for X-ray diffraction (Fig. 2) were prepared by slow evaporation (for $\mathbf{1_o}$) and vapor exchange (for $\mathbf{2_o}$). Attempts to obtain crystals for $\mathbf{3_o}$ failed, and only the X-ray structure of a dichlorinated neutral derivative ($\mathbf{3_oCl_2}$) was obtained after chemical oxidation experiments (Fig. S1d, S2d and S7). At the solid state, molecule $\mathbf{1_o}$ establishes C-H···π interactions in a herringbone arrangement with a distance of 3.45(11) Å and an angle of ~50° (Fig. 2c). Molecule $\mathbf{2_o}$ forms pillars through π-π stacks (Fig. 2h-g) with an interplanar distance of 3.34(15) Å and a relative orientation of ~80° (Fig. 2f).

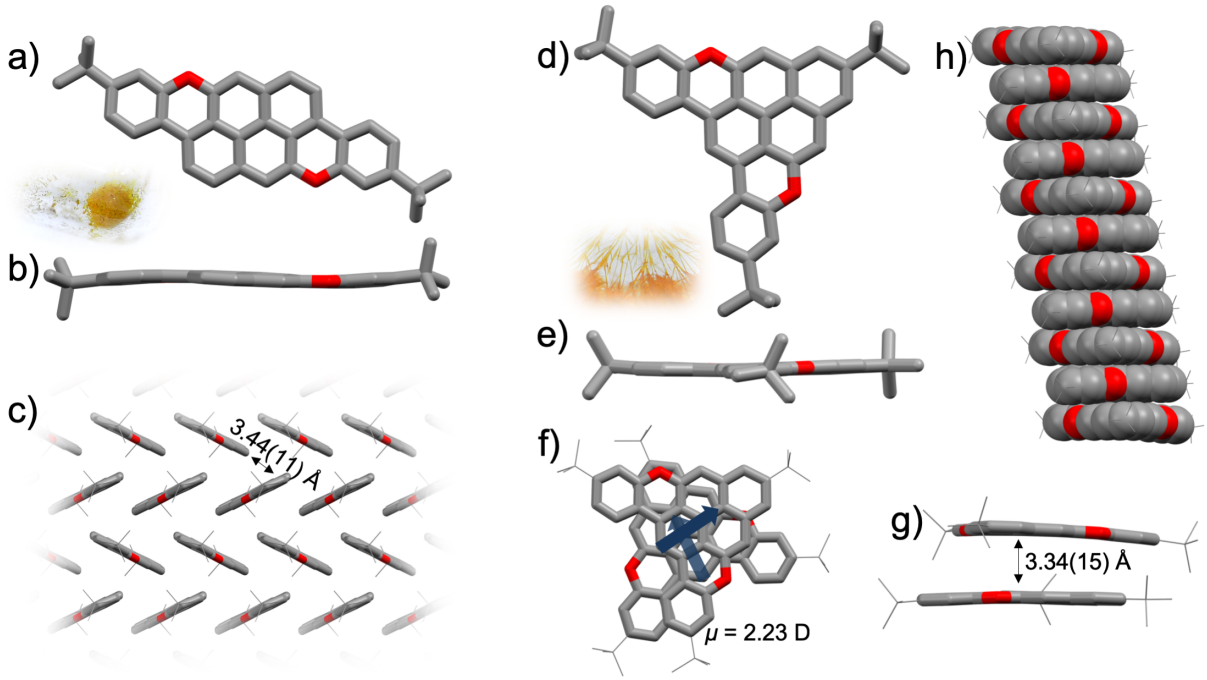

Fig. 2. X-Ray crystal structures of **1o** and **2o**. a) Top-view, b) side-view and c) packing mode of $\mathbf{1_o}$. d) Top-view, e) side-view and h) packing mode of $\mathbf{2_o}$. f,g) Details related to the stacking mode of $\mathbf{2_o}$, top- and side-view. Space groups: $P2_1/I$ ($\mathbf{1_o}$) and $C2/c$ ($\mathbf{2_o}$). Atom colors: red O, gray C.

Molecules $\mathbf{1_o}$, $\mathbf{2_o}$ and $\mathbf{3_o}$ present the lowest electronic transitions at 466, 487 and 506 nm, respectively (Table 1, Fig. 3 and S8), with the strongest absorptivity found for $\mathbf{1_o}$ and $\mathbf{3_o}$. As displayed by TD-DFT calculations (Tables S20-S22, Fig. S47 and S49), these bands are attributed to π–π^* transitions. Comparison between absorption profiles (in THF) of O-doped PAH $\mathbf{1_o}$ and the (only) previously reported full-carbon compound $\mathbf{1_c}$, revealed a blue-shifted lowest energy absorption maximum (from 586 to 466 nm for $\mathbf{1_c}$ and $\mathbf{1_o}$, respectively, Fig. S10). The increase in the optical band gap is caused by replacement of two benzenoid rings with (slightly) anti-aromatic pyrano rings, which causes an increase in the LUMO level (from DFT calculations: E_{LUMO} = −2.80 and −1.80 eV for $\mathbf{1_c}$ and $\mathbf{1_o}$, respectively), while the HOMO level is barely affected (E_{HOMO} = −4.85 and −4.72 eV for $\mathbf{1_c}$ and $\mathbf{1_o}$, respectively). Emission profiles for $\mathbf{1_o}$, $\mathbf{2_o}$ and $\mathbf{3_o}$ displayed mirroring luminescence profiles with narrow Stokes' shifts (4, 9 and 18 nm, respectively), high quantum yields (Φ_{fl} = 93, 88 and 68%, respectively) and short lifetimes (τ = 2.2, 6.2 and 6.2 ns, respectively).

Table 1. Optoelectronic properties of $\mathbf{1_o}$–$\mathbf{3_o}$ in air-equilibrated THF. Half-wave potentials ($E_{1/2}$) were determined by CV (THF, 0.1 M *n*-Bu_4NPF_6) and referenced versus Fc^+/Fc couple.

Molecule	λ_{abs} [nm]	λ_{em} [nm]	ϕ_{fl}[a] [%]	E_{00}[b] [eV]	E_{ac}^{red}[c] [V]	$E_{1/2}^{ox1}$ [V]	$E_{1/2}^{ox2}$ [V]	E_{HOMO}[e] [eV]	E_{LUMO}[f] [eV]
$\mathbf{1_o}$	466	470	93	2.64	−2.54	0.10	0.54	−4.90	−2.26
$\mathbf{2_o}$	487	496	88	2.50	−2.42	0.29	0.72[d]	−5.09	−2.59
$\mathbf{3_o}$	506	524	68	2.36	−2.02	0.15	0.54	−4.95	−2.59

[a]ϕ_{fl} measured by optical dilute method and Coumarin 153 as reference. [b]Optical bandgap. [c]From the cathodic peak of an irreversible process. [d]From the anodic peak of an irreversible process. [e]Formal potential of Fc^+/Fc couple is assumed to be −4.8 eV *vs* vacuum. [f]Calculated using E_{00}.

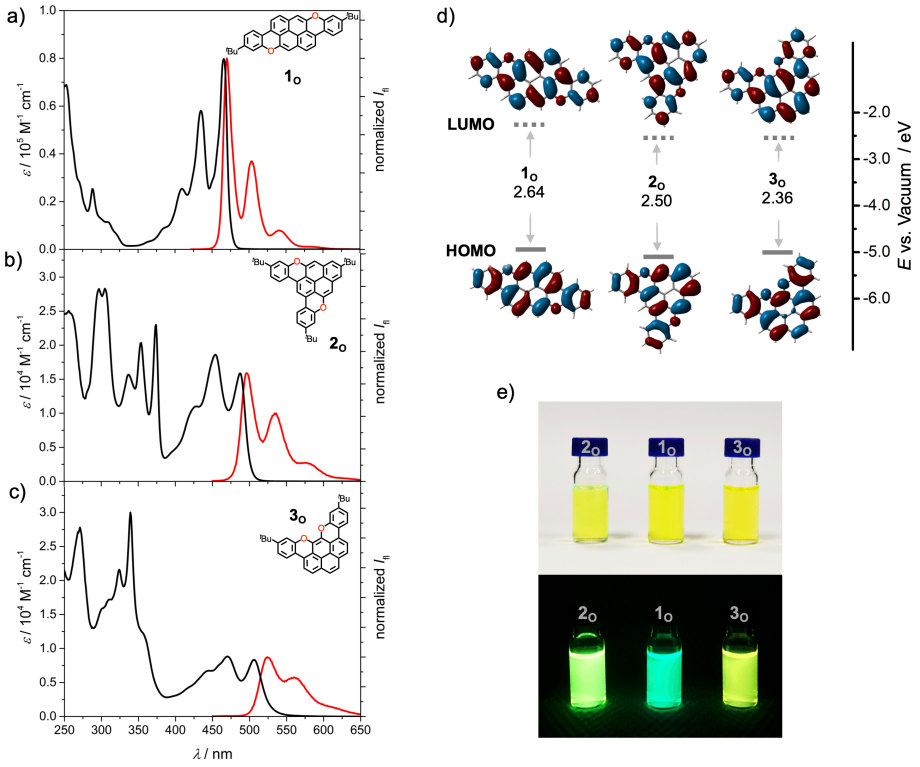

Fig. 3. a–c) UV-Vis absorption (black) and emission (red) spectra for $\mathbf{1_o}$–$\mathbf{3_o}$ in THF at room temperature. d) FMO energies obtained by CV (full) and E_{00} (dashed) along with orbital densities calculated at the B3LYP/6-31(d,p) level of theory (isoval: 0.02 a.u.); the optical bandgap shrinks following the order $\mathbf{1_o}$>$\mathbf{2_o}$>$\mathbf{3_o}$. e) Absorption and emission colours for $\mathbf{1_o}$–$\mathbf{3_o}$ in THF at r.t.

Cyclic voltammetry (CV) was used to assess the redox properties in THF (Table 1, Fig. S11-S13). The CV profiles of $\mathbf{1_o}$ and $\mathbf{3_o}$ feature two reversible oxidation couples (0.10 and 0.54 V for $\mathbf{1_o}$ and 0.15 and 0.54 V for $\mathbf{3_o}$), whereas only one reversible oxidation event was detected for $\mathbf{2_o}$ at 0.29 V, together with an irreversible process at 0.72 V. Only irreversible reduction waves were observed in the redox window of THF. Comparing the diffusion coefficients measured for $\mathbf{1_o}$, $\mathbf{2_o}$ and $\mathbf{3_o}$ by DOSY-NMR (1.10×10^{-5}, 9.89×10^{-6} and 1.11×10^{-5} cm^2 s^{-1}, respectively) with those obtained from the first cathodic events (1.24×10^{-5}, 9.55×10^{-6} and 1.13×10^{-5} cm^2 s^{-1} measured at 0.18, 0.34 and 0.20 V, respectively), we could assert that the first oxidative waves correspond to the formation of the radical cation species ($\mathbf{1_o}^{\bullet+}$, $\mathbf{2_o}^{\bullet+}$ and $\mathbf{3_o}^{\bullet+}$, see Section 5 in the SI). These findings suggest that all oxidation states are likely accessible by titration with tris(4-bromophenyl)ammoniumyl hexafluoroantimonate ($BAHA_F$), a one-e^- oxidant (E^{red} = 0.70 V vs Fc/Fc^+).[19]

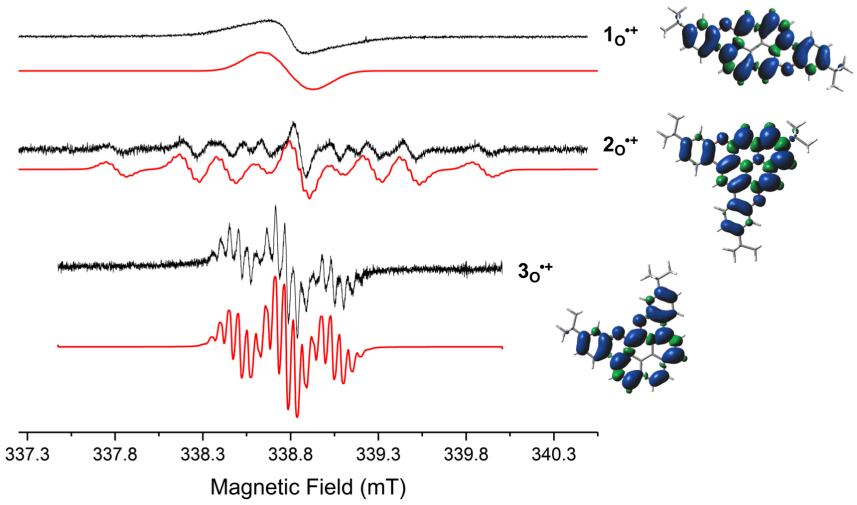

Fig. 4. X-band CW-EPR spectra (-) and simulations (–) of radical cations $\mathbf{1_o}^{\bullet+}$, $\mathbf{2_o}^{\bullet+}$ and $\mathbf{3_o}^{\bullet+}$ in THF solutions as generated with $BAHA_F$ (left). Iso-spin density distribution maps for the spin density value of 0.002 electron/bohr by DFT at the UB3LYP/EPR-II level of theory for the radical cations (right).

The effects of oxidation are particularly apparent in EPR spectra if unpaired electrons are formed. Titration of one eq. of $BAHA_F$ into solutions of $\mathbf{1_o}$, $\mathbf{2_o}$ and $\mathbf{3_o}$ gave radical cations $\mathbf{1_o}^{\bullet+}$, $\mathbf{2_o}^{\bullet+}$ and $\mathbf{3_o}^{\bullet+}$, the latter exhibiting X-band CW-EPR signals characteristic of S = 1/2 electron spin systems (Fig. 3). The isotropic g_{iso} and $^{H}a_{iso}$ values show agreement with those estimated from theory (Table S5). Upon

further additions of $BAHA_F$ (>1 eq.), the intensity of the EPR signals decreased until complete disappearance (>2 eq.), and this coincided with the emergence of the EPR signal of $BAHA_F$. For instance, closed-shell, EPR-silent, cations $\mathbf{1_o}^{2+}$ and $\mathbf{3_o}^{2+}$ are obtained in the case of $\mathbf{1_o}$ and $\mathbf{3_o}$ (Fig. S35). Given the irreversibility of the second oxidation process for $\mathbf{2_o}$, we did not perform any EPR characterization for this molecule in the presence of an excess of $BAHA_F$. To shed further light on the properties of the oxidized species, we also performed UV-Vis-NIR spectroelectrochemical (Fig. S17-S20) and spectrophotometric titration experiments with both BAHA (magic blue) and $BAHA_F$ (Fig. 5 and S21-S24). In all cases, the absorption spectra readily underwent dramatic changes, evidencing the progressive disappearance of the electronic transitions at 410-510 nm and the simultaneous appearance of new red-shifted bands in the NIR spectral region, typical of radical cations species. We further attempted to characterize the dications in solution by ^{1}H-NMR spectroscopy (Fig. S25-S28). While we observed the disappearance of signals from the neutral species upon addition of BAHA, accompanied by presence of new proton resonances, the interpretation was complicated by the evident loss of intensity, presumably due to the strong tendency of the oxidized species to aggregate (Fig. S28). Moreover, all attempts to obtain single crystals suitable for X-ray diffraction of the chemically-oxidized species were unsuccessful.

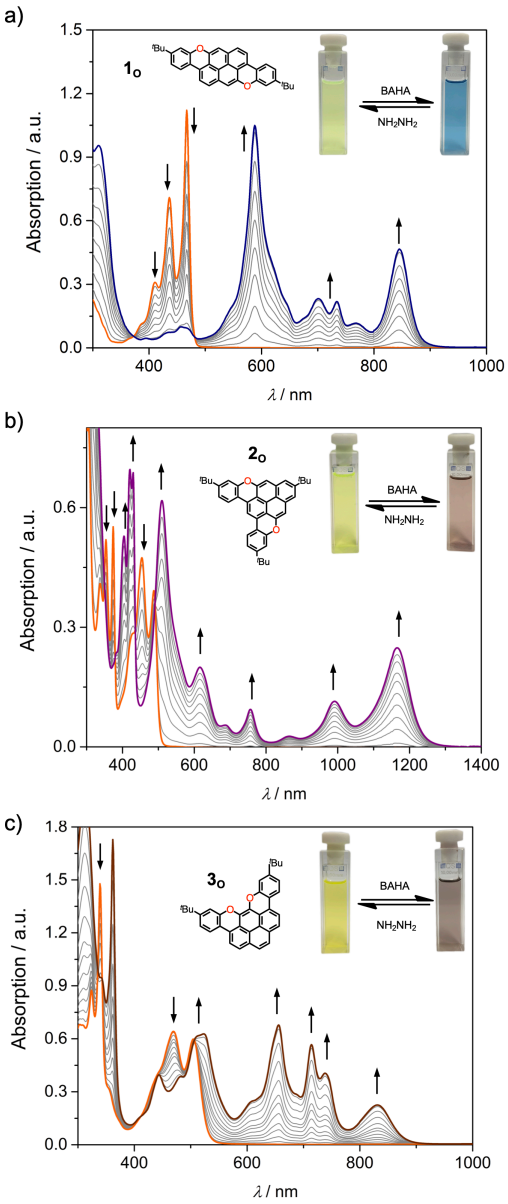

Fig. 5. UV-Vis-NIR spectra obtained by titration of a) $\mathbf{1_o}$, b) $\mathbf{2_o}$ and c) $\mathbf{2_o}$ with BAHA (magic blue) in dry CH_2Cl_2 at 298 K.

The formation of the cationic species was further corroborated by DFT calculations and their aromaticity was probed by nucleus-independent chemical shift (NICS) and anisotropy of the induced current density (AICD) analyses (SI, Section 11).[20] $NICS(1)_{zz}$ values (Fig. S54-S57) for the pyrano rings show antiaromatic character (+12.76, +10.93 and +14.66 ppm for $\mathbf{1_o}$, $\mathbf{2_o}$ and $\mathbf{2_o}$, respectively), while oxidation by one-electron results in that ring being essentially non-aromatic (−1.18, +0.73 and +0.30 ppm, respectively), and double oxidation gives pyrylium rings with aromatic character (−18.06,

−6.54 and −17.11 ppm, respectively) similar to the all-carbon neutral PAH counterparts $\mathbf{1_c}$–$\mathbf{3_c}$ (Fig. S58-S59). In contrast to typical C-O single bond (1.43 Å), the new formed C-O bonds (Fig. S44-S46) are substantially shorter (1.37 Å) in the neutral $\mathbf{1_o}$–$\mathbf{3_o}$ species, suggesting that the O-PAHs lone-pair electrons contribute in the *π*-electron interactions. The C-O bonds were observed to shorten even further in the calculated oxidized O-PAHs (1.35 Å for the radical cations and 1.33-1.34 Å for the dications). TD-DFT simulations (Tables S25-S30, Fig. S50) of the UV-vis absorption envelop resembled that observed experimentally for the oxidized species.

We turned our attention to the electrocrystallisation technique[21] to grow crystals of the cations suitable for X-ray diffraction, performing electrooxidation experiments (SI, Section 8). Triclinic shiny black crystals containing salts of mixed-valence (MV) complexes for O-doped PAHs $\mathbf{1_o}$ and $\mathbf{3_o}$ were obtained in THF with *n*-Bu_4NPF_6 and *n*-Bu_4NClO_4 as electrolytes, respectively (Fig. 6). While the former electro-crystallizes in an asymmetric unit containing ten crystallographically-independent O-doped molecules, six PF_6^- anions and 16 solvent molecules, $(\mathbf{1_o})_{10}(PF_6)_6\cdot(THF)_{16}$, the latter depicts three independent O-PAHs, two ClO_4^- anions, one THF and half H_2O molecules, $(\mathbf{3_o})_3(ClO_4)_2\cdot THF\cdot{}^1/_2H_2O$. All attempts to grow suitable crystals containing oxidized species of $\mathbf{2_o}$ for X-ray analyses failed.

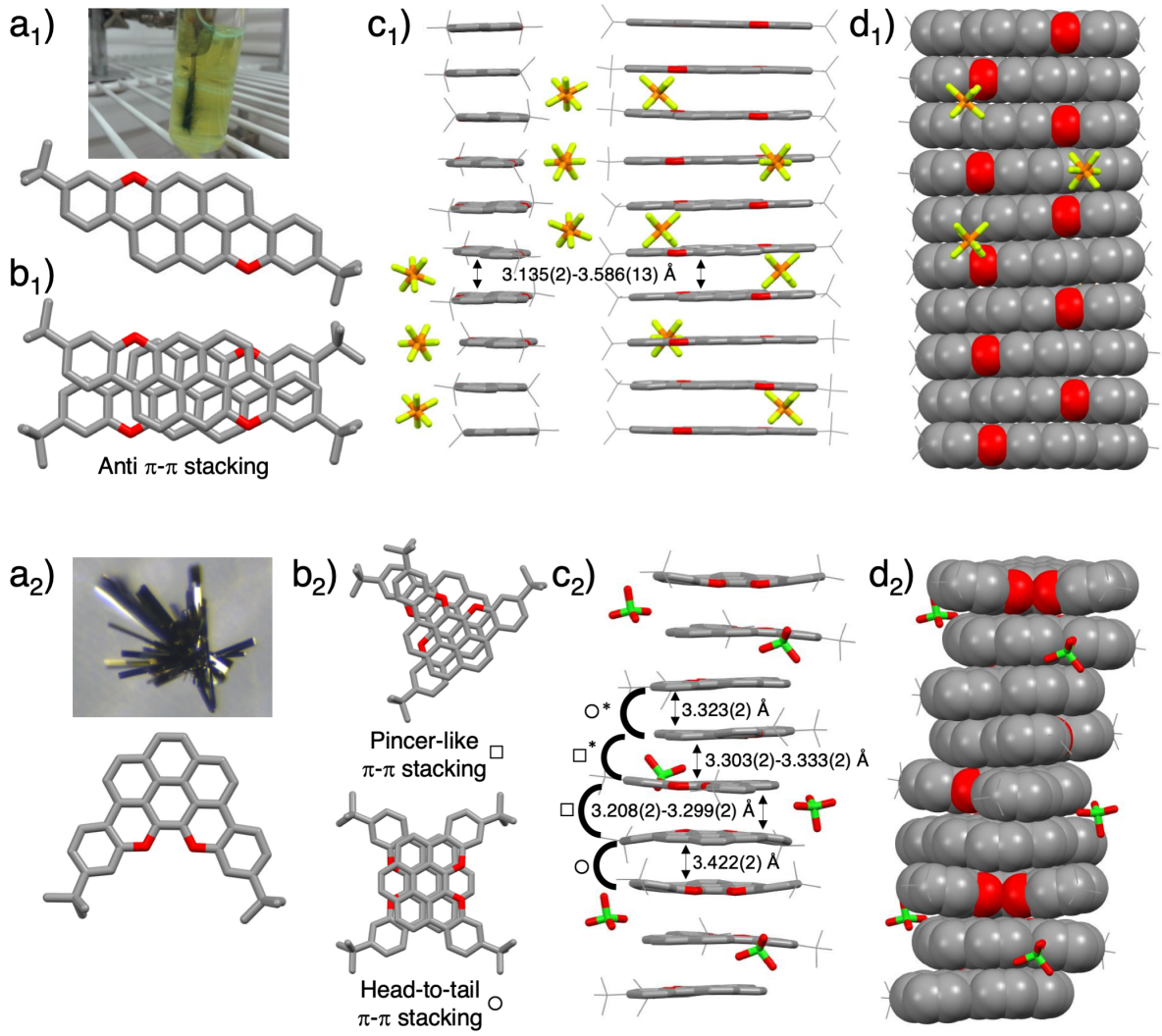

Fig. 6. X-ray crystals structures for MV complexes $(\mathbf{1_o})_{10}(PF_6)_6\cdot(THF)_{16}$ (top, *P*-1) and $(\mathbf{3_o})_3(ClO_4)_2\cdot THF\cdot{}^1/_2H_2O$ (down, *P*-1), solvent molecules omitted for clarity. a) Morphology of the crystals and X-ray structure of the relevant isolated O-doped molecule, b) *π–π* stacking mode, c-d) solid-state columnar *π–π* stacks. *For the MV complexes of $\mathbf{3_o}$, each stacking mode between two **3o** molecules gives rise to two different off-set arrangements. Atom colors: red O, gray C., green Cl, yellow F, orange P.

Looking at organization at the solid state of $(\mathbf{1_o})_{10}(PF_6)_6\cdot(THF)_{16}$ (Fig. $6a_1$-d_1), one can clearly evidence the presence of a columnar arrangement in which the molecules organize antiparallely (Fig. $6b_1$), with an average interplanar spacing of 3.33(7) Å (shortest distance between ring centroids of 3.367(12) Å with a lateral slippage of 0.83 Å). The PF_6^- counterions are evenly intercalated in the channels (Fig. $4c_1$) together with solvent THF molecules. Similarly, in the crystal of $(\mathbf{3_o})_3(ClO_4)_2\cdot THF\cdot{}^1/_2H_2O$ (Fig. $6a_2$-d_2), molecule $\mathbf{3_o}$ segregates in *π–π* stacks (*π–π* distances from 3.21 to 3.42 Å, Fig. $6c_2$), with ClO_4^- anions and solvent molecules intercalating between different

stacks. In this crystal, two stacking modes are present: a pincer-like stack (Fig. 6b$_2$, top), in which two independent molecules are facing to each other in an antiparallel fashion with a relative angle of about 90°, and a head-to-tail arrangement (Fig. 6b$_2$, bottom), where two molecules antiparallely stack. In both MV complexes, all O-doped PAHs show very similar bond lengths (SI, Table S4) and short interplanar π–π distances. These structures are consistent with a material in which the charge is delocalized over the stacks.[22] A MV salt would form a partially filled band structure, providing the conduction carrier.

As crystals for $(\mathbf{1_o})_{10}(PF_6)_6\cdot(THF)_{16}$ were extremely fragile, we used $(\mathbf{3_o})_3(ClO_4)_2\cdot THF\cdot{}^1/_2H_2O$ to probe the electronic properties of the organic salts. We first performed variable temperature (VT) X-band CW-EPR investigations (Fig. 7a). The EPR spectra are constituted by what appears to be a (medium polarized) conduction electron spin resonance line, most likely associated with delocalization of spin density along the longitudinal axis of the π-stacking architecture. This behavior has been observed in systems showing metal to insulator/semiconductor transition.[23] As the intensity of the EPR signal decreases when the temperature is lowered, an Arrhenius plot has been used to interpret the VT-dependent EPR behavior (Fig. 7a-b). The linear portion of the trend at low temperature was fitted to a line of equation $f({}^1/_T) = -476\,{}^1/_T + 8.77$ and an activation energy (E_a) of 4.1×10^{-2} eV was obtained in good agreement with the value derived from single-crystal conductivity measurements.

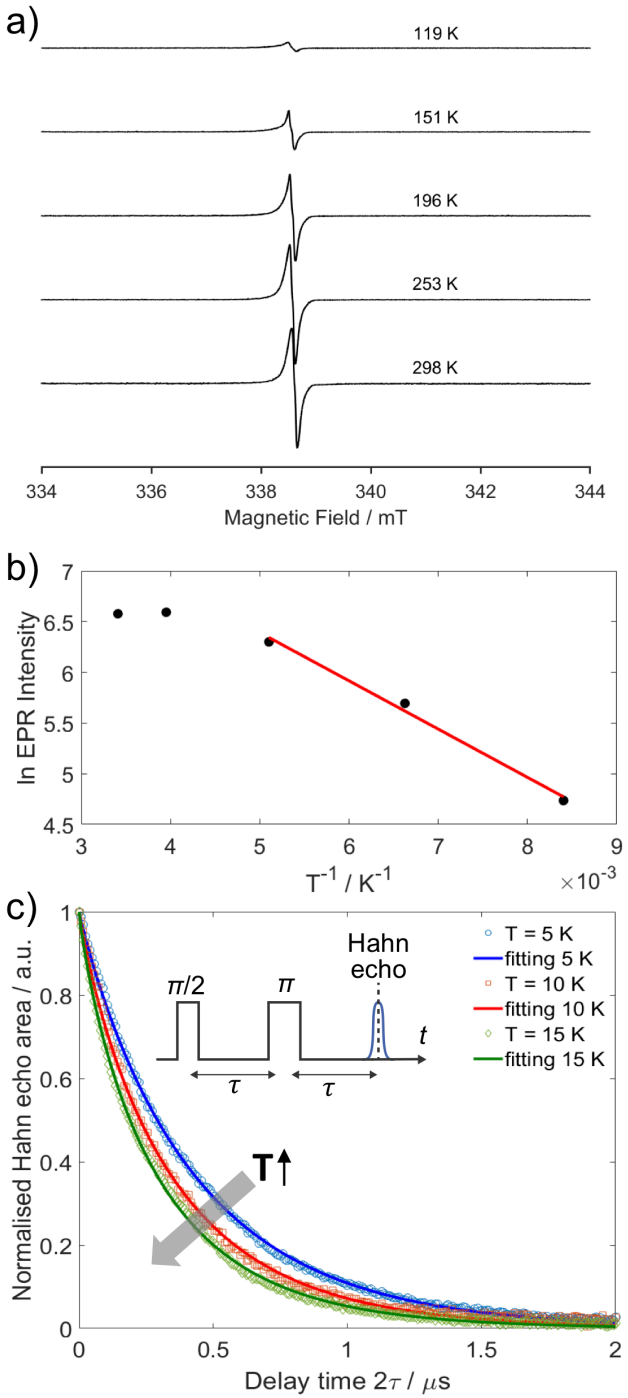

Fig. 7. a) X-band CW-EPR VT-spectra of crystals $(\mathbf{3_o})_3(ClO_4)_2 \cdot THF \cdot {}^1/_2H_2O$ between 298 K and 119 K at 10 kHz field modulation frequency; b) natural logarithm (•••) of the EPR intensities versus 1/T Arrhenius plot, the fitting (–) give R^2 = 0.9933; c) 2-pulse Hahn echo decay measured at 15 K (–), 10 K (–) and 5 K (–). The pulse sequence adopted to generate a primary electron spin echo is shown as an inset. Microwave pulse lengths of π = 120 ns were used to suppress any potential proton-electron spin modulation. (d) Echo-detected saturation recovery experiment at 15 K (green trace), 10 K (red trace) and 5 K (blue trace). The pulse sequence adopted is shown as an inset, where π = 48 ns, τ = 248 ns and the delay time T is variable.

Relaxation studies were also performed at of 5, 10 and 15 K to calculate the phase memory time T_m (*i.e.*, transversal relaxation or

spin-spin relaxation time T_2, Fig. 7c). Already at 20 K no Hahn echo was detected when using a primary $\pi/2-\pi-\pi$ pulse sequence, even when shortening the inter-pulse delay, τ, to the minimum. A fast T_m value of 0.43 μs was measured at 5 K, which rapidly decreases to 0.34 μs and 0.29 μs at 10 K and 15 K, respectively. Notably, solid-state T_m values are ten times lower than those measured in frozen THF for radical cation $\mathbf{3_o}^{\bullet+}$, *i.e.* 4 μs at 5 K (Fig. S37). Overall, these observations suggest that fast spin-spin relaxation routes occur in the crystal due to the stacking of the paramagnetic radical cations. Similarly, short relaxation time T_1 (or longitudinal spin-lattice relaxation time) was measured (Fig. S37). A decrease of the T_1 value was also observed as a function of the temperature (0.21 ms at 5 K, 0.07 ms at 10 K and 0.05 ms at 15 K), which is 120 times lower than the T_1 value (25 ms) measured for $\mathbf{3_o}^{\bullet+}$ in solution. The dramatic lowering of T_1 further corroborates the presence of the ordered crystal lattice in the electrochemically-growth solid material.

I-V curves of single crystals of $(\mathbf{3_o})_3(ClO_4)_2\cdot THF\cdot{}^1/_2H_2O$ exhibit a typical semiconductor behavior with a sigmoidal shape rather than a linear behavior, consistent with the observed temperature dependence of the conductivity (Fig. 8a-b).[24] The conductivity (σ) was calculated in the ohmic region (σ_{ohmic}), *i.e.*, around zero bias and, as an extension, in the non-ohmic ($\sigma_{non-ohmic}$) activated regime at higher bias values. Considering that organic materials are typically poorly conductive semiconductors (σ <10^{-6} S cm^{-1} at 300 K) or just insulators,[25] our mixed-valence crystalline complexes exhibit high conductivity at room temperature (σ_{ohmic} = 8.8 × 10^{-5} and 3.7 × 10^{-3} S cm^{-1}; $\sigma_{non-ohmic}$ = 2.4 × 10^{-4} and 5.1 × 10^{-3} S cm^{-1} for crystals α and β, respectively). Exceptions include crystalline organic conductors and superconductors based on electron donors (such as TTF) and acceptors (such as TCNQ),[26] some organic and inorganic radicals,[27] and some metal-organic frameworks (MOFs).[28]

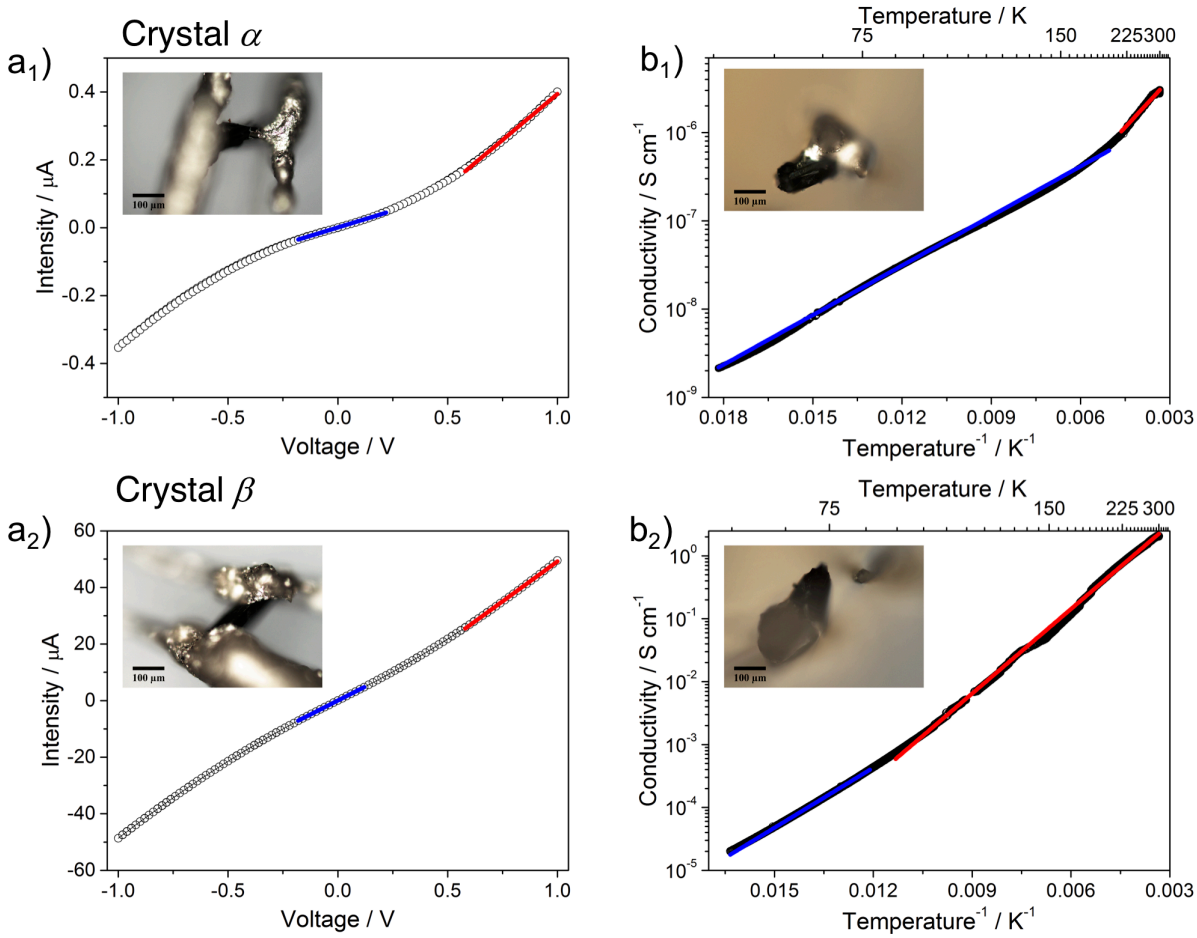

Fig. 8. Device and electrical response of two crystals (α and β) of $(\mathbf{3_o})_3(ClO_4)_2 \cdot THF \cdot {}^1/_2H_2O$: a) I-V curve (•••) at 300K with the ohmic linear fit (–) and non-ohmic fit (–). For **crystal α**: The ohmic fit (R^2 = 0.99752) gives a slope of 1.98±0.02 × 10^{-7} Ω^{-1} and a y-intercept value of 9±2 × 10^{-10} A; non-ohmic fit (R^2 = 0.99752) gives a slope of 5.43±0.01 × 10^{-7} Ω^{-1} and a y-intercept value of −1.48±0.003 × 10^{-7} A. For **crystal β**: The ohmic fit (R^2 = 0.99998) gives a slope of 3.943±0.005 × 10^{-5} Ω^{-1} and a y-intercept value of 2±5 × 10^{-9} A; non-ohmic fit (R^2 = 0.99957) gives a slope of 5.46±0.02 × 10^{-5} Ω^{-1} and a y-intercept value of −7.26±0.0015 × 10^{-6} A. b) Arrhenius plot of the conductivity *vs.* temperature (•••) together with the linear fits (–, –) in the low- and high-temperature regimes. Conductivity values calculated at high ($\sigma_{0,HT}$) and low ($\sigma_{0,LT}$) temperatures and associated activation energies ($E_{a,HT}$ and $E_{a,LT}$). For **crystal α:** $\sigma_{0,HT}$ = 5.50±0.05 S cm^{-1} and $E_{a,HT}$ = 72.0±0.6 meV (R^2 = 0.99359); $\sigma_{0,LT}$ = 4.92±0.12 × 10^{-6} S cm^{-1} and $E_{a,LT}$ = 37.15±0.14 meV (R^2 = 0.99915); for **crystal β:** $\sigma_{0,HT}$ = 70.0±0.5 S cm^{-1} and $E_{a,HT}$ = 80.21±0.09 meV (R^2 = 0.99817); $\sigma_{0,LT}$ = 2.81±0.08 × 10^{-6} S cm^{-1} and $E_{a,LT}$ = 63.11±0.07 meV (R^2 = 0.99967). Insets: top view (a) and lateral view (b) of the devices.

Conclusions

In summary, we have developed an efficient synthesis for the construction of O-embedded PAHs. This approach consists in longitudinal or latitudinal extension of dihalogenated pyrenes, that coupled with phenol moieties can be planarized through Pummerer oxidative ring-closure (CuO in $PhNO_2$). Electrochemical and chemical

oxidation investigations showed that the cations of O-PAHs can be easily accessed, prompting us to perform electrocrystallisation experiments to form organic MV crystals. The organic salts organize in columns at the solid state, depicting a strong electron delocalization along the longitudinal axis of the π-stacks. Electric measurements of single crystals of the MV salts exhibited a semiconducting behavior with relatively high conductivity at room temperature, further supporting the idea for which the heteroatom approach is a viable route for empowering PAHs and nanographenes with a broad spectrum of semiconducting properties and high charge mobilities.

References

[1] a) L. Chen, Y. Hernandez, X. Feng, K. Müllen, *Angew. Chem. Int. Ed.* **2012**, *51*, 7640-7654; b) A. Narita, X. Y. Wang, X. Feng, K. Müllen, *Chem. Soc. Rev.* **2015**, *44*, 6616-6643; c) Y. Segawa, H. Ito, K. Itami, *Nat. Rev. Mat.* **2016**, *1*, 15002.

[2] a) L. Zhang, Y. Cao, N. S. Colella, Y. Liang, J. L. Bredas, K. N. Houk, A. L. Briseno, *Acc. Chem. Res.* **2015**, *48*, 500-509; b) T. B. Schon, B. T. McAllister, P.-F. Li, D. S. Seferos, *Chem. Soc. Rev.* **2016**, *45*, 6345-6404; c) P. Mayorga Burrezo, W. Zeng, M. Moos, M. Holzapfel, S. Canola, F. Negri, C. Rovira, J. Veciana, H. Phan, J. Wu, C. Lambert, J. Casado, *Angew. Chem. Int. Ed.* **2019**, *58*, 14467-14471.

[3] a) X. Wang, G. Sun, P. Routh, D. H. Kim, W. Huang, P. Chen, *Chem. Soc. Rev.* **2014**, *43*, 7067-7098; b) M. Stępień, E. Gońka, M. Żyła, N. Sprutta, *Chem. Rev.* **2017**, *117*, 3479-3716; c) R. Szucs, P. A. Bouit, L. Nyulaszi, M. Hissler, *ChemPhysChem* **2017**, *18*, 2618-2630; d) M. Hirai, N. Tanaka, M. Sakai, S. Yamaguchi, *Chem. Rev.* **2019**, *119*, 8291-8331.

[4] a) S. Yamaguchi, in *Chemical Science of π-Electron Systems*, 10.1007/978-4-431-55357-1_21 (Eds.: T. Akasaka, A. Osuka, S. Fukuzumi, H. Kandori, Y. Aso), Springer Japan, Tokyo, **2015**, pp. 363-377; b) D. Bonifazi, F. Fasano, M. M. Lorenzo-García, D. Marinelli, H. Oubaha, J. Tasseroul, *Chem. Commun.* **2015**, *51*,

15222–15236; c) H. Helten, *Chem. – Eur. J.* **2016**, *22*, 12972–12982; d) M. M. Morgan, W. E. Piers, *Dalton Trans.* **2016**, *45*, 5920–5924; e) A. John, M. Bolte, H. W. Lerner, M. Wagner, *Angew. Chem. Int. Ed.* **2017**, *56*, 5588–5592; f) J. M. Farrell, D. Schmidt, V. Grande, F. Würthner, *Angew. Chem. Int. Ed.* **2017**, *56*, 11846–11850; g) R. J. Kahan, D. L. Crossley, J. Cid, J. E. Radcliffe, M. J. Ingleson, *Angew. Chem. Int. Ed.* **2018**, *57*, 8084–8088; h) H. Noda, Y. Asada, M. Shibasaki, N. Kumagai, *J. Am. Chem. Soc.* **2019**, *141*, 1546–1554; i) M. Vanga, R. A. Lalancette, F. Jakle, *Chem. – Eur. J.* **2019**, *25*, 10133–10140.

[5] a) D. B. Granger, Y. Mei, K. J. Thorley, S. R. Parkin, O. D. Jurchescu, J. E. Anthony, *Org. Lett.* **2016**, *18*, 6050–6053; b) Y. S. Park, D. J. Dibble, J. Kim, R. C. Lopez, E. Vargas, A. A. Gorodetsky, *Angew. Chem. Int. Ed.* **2016**, *55*, 3352–3355; c) D. Lehnherr, J. M. Alzola, C. R. Mulzer, S. J. Hein, W. R. Dichtel, *J. Org. Chem.* **2017**, *82*, 2004–2010; d) L. Ji, A. Friedrich, I. Krummenacher, A. Eichhorn, H. Braunschweig, M. Moos, S. Hahn, F. L. Geyer, O. Tverskoy, J. Han, C. Lambert, A. Dreuw, T. B. Marder, U. H. F. Bunz, *J. Am. Chem. Soc.* **2017**, *139*, 15968–15976; e) Z. Zeng, H. Jin, K. Sekine, M. Rudolph, F. Rominger, A. S. K. Hashmi, *Angew. Chem. Int. Ed.* **2018**, *57*, 6935–6939; f) P. Karak, C. Dutta, T. Dutta, A. L. Koner, J. Choudhury, *Chem. Commun.* **2019**, *55*, 6791–6794; g) U. H. F. Bunz, J. Freudenberg, *Acc. Chem. Res.* **2019**, *52*, 1575–1587; h) C. L. Deng, J. P. Bard, L. N. Zakharov, D. W. Johnson, M. M. Haley, *Org. Lett.* **2019**, *21*, 6427–6431; i) B. L. Hu, C. An, M. Wagner, G. Ivanova, A. Ivanova, M. Baumgarten, *J. Am. Chem. Soc.* **2019**, *141*, 5130–5134; j) J. P. Mora-Fuentes, A. Riaño, D. Cortizo-Lacalle, A. Saeki, M. Melle-Franco, A. Mateo-Alonso, *Angew. Chem. Int. Ed.* **2019**, *58*, 552–556.

[6] a) D. Wu, W. Pisula, M. C. Haberecht, X. Feng, K. Müllen, *Org. Lett.* **2009**, *11*, 5686–5689; b) S. Shinamura, E. Miyazaki, K. Takimiya, *J. Org. Chem.* **2010**, *75*, 1228–1234; c) K. P. Rao, M. Kondo, R. Sakamoto, T. Kusamoto, M. Nishikawa, S. Kume, M. Nihei, H. Oshio, H. Nishihara, *Chem. – Eur. J.* **2011**, *17*, 14010–14019; d) M. Nakano, K. Niimi, E. Miyazaki, I. Osaka, K.

Takimiya, *J. Org. Chem.* **2012**, *77*, 8099-8111; e) B. Vanveller, D. Robinson, T. M. Swager, *Angew. Chem. Int. Ed.* **2012**, *51*, 1182-1186; f) S. Wang, B. Lv, Q. Cui, X. Ma, X. Ba, J. Xiao, *Chem. - Eur. J.* **2015**, *21*, 14791-14796; g) D. Stassen, N. Demitri, D. Bonifazi, *Angew. Chem. Int. Ed.* **2016**, *55*, 5947-5951; h) T. Miletić, A. Fermi, I. Orfanos, A. Avramopoulos, F. De Leo, N. Demitri, G. Bergamini, P. Ceroni, M. G. Papadopoulos, S. Couris, D. Bonifazi, *Chem. - Eur. J.* **2017**, *23*, 2363 –2378; i) A. Berezin, N. Biot, T. Battisti, D. Bonifazi, *Angew. Chem. Int. Ed.* **2018**, 57, 8942-; j) A. Sciutto, A. Fermi, A. Folli, T. Battisti, J. Beames, D. Murphy, D. Bonifazi, *Chem. - Eur. J.* **2017**, 24, 4382-; l) A. Sciutto, A. Berezin, M. Lo Cicero, T. Miletic, A. Stopin, D. Bonifazi, *J. Org. Chem.* **2018**, *83*, 13787-; m) C. Li, L. Zhu, W. Liang, R. Su, J. Yin, Y. Hu, Y. Lan, D. Wu, J. You, *Chem. Sci.* **2019**, *10*, 7274-7280; n) S. Dong, T. Y. Gopalakrishna, Y. Han, H. Phan, T. Tao, Y. Ni, G. Liu, C. Chi, *J. Am. Chem. Soc.* **2019**, *141*, 62-66.

[7] a) P. Ruffieux, S. Wang, B. Yang, C. Sánchez-Sánchez, J. Liu, T. Dienel, L. Talirz, P. Shinde, C. A. Pignedoli, D. Passerone, T. Dumslaff, X. Feng, K. Müllen, R. Fasel, *Nature* **2016**, *531*, 489-492; b) X. Wang, F. Zhang, K. S. Schellhammer, P. Machata, F. Ortmann, G. Cuniberti, Y. Fu, J. Hunger, R. Tang, A. A. Popov, R. Berger, K. Müllen, X. Feng, *J. Am. Chem. Soc.* **2016**, *138*, 11606-11615; c) M. Numano, N. Nagami, S. Nakatsuka, T. Katayama, K. Nakajima, S. Tatsumi, N. Yasuda, T. Hatakeyama, *Chem. - Eur. J.* **2016**, *22*, 11574-11577; d) M. Fingerle, C. Maichle-Mössmer, S. Schundelmeier, B. Speiser, H. F. Bettinger, *Org. Lett.* **2017**, *19*, 4428-4431.

[8] a) F. Pina, M. J. Melo, C. A. Laia, A. J. Parola, J. C. Lima, *Chem. Soc. Rev.* **2012**, *41*, 869-908; b) F. Pina, *Dyes Pigm.* **2014**, *102*, 308-314.

[9] a) O. Anamimoghadam, M. D. Symes, D. L. Long, S. Sproules, L. Cronin, G. Bucher, *J. Am. Chem. Soc.* **2015**, *137*, 14944-14951; b) C. M. Wehrmann, R. T. Charlton, M. S. Chen, *J. Am. Chem. Soc.* **2019**, *141*, 3240-3248; c) Y. Wang, S. Qiu, S. Xie, L. Zhou,

Y. Hong, J. Chang, J. Wu, Z. Zeng, *J. Am. Chem. Soc.* **2019**, *141*, 2169–2176.

[10] a) T. S. Balaban, A. T. Balaban, in *Six-membered Hetarenes with one Chalcogen, Vol. 14* (Ed.: E. J. Thomas), Georg Thieme Verlag, Stuttgart, **2003**, pp. 11—200; b) J. Yin, M. Tan, D. Wu, R. Jiang, C. Li, J. You, *Angew. Chem. Int. Ed.* **2017**, *56*, 13094–13098.

[11] a) E. Clar, *Chem. Ber.* **1943**, *76*, 328–333; b) D. Lungerich, O. Papaianina, M. Feofanov, J. Liu, M. Devarajulu, S. I. Troyanov, S. Maier, K. Amsharov, *Nat. Commun.* **2018**, *9*, 4756.

[12] a) C. Reus, M. P. Lechner, M. Schulze, D. Lungerich, C. Diner, M. Gruber, J. M. Stryker, F. Hampel, N. Jux, R. R. Tykwinski, *Chem. - Eur. J.* **2016**, *22*, 9097–9101; b) K. Sbargoud, M. Mamada, T. Jousselin-Oba, Y. Takeda, S. Tokito, A. Yassar, J. Marrot, M. Frigoli, *Chem. - Eur. J.* **2017**, *23*, 5076–5080.

[13] J. Hwang, M. Pototschnig, R. Lettow, G. Zumofen, A. Renn, S. Götzinger, V. Sandoghdar, *Nature* **2009**, *460*, 76–80.

[14] P. Siyushev, G. Stein, J. Wrachtrup, I. Gerhardt, *Nature* **2014**, *509*, 66–70.

[15] B. Yang, J. B. Trebbia, R. Baby, P. Tamarat, B. Lounis, *Nat. Photon.* **2015**, *9*, 658–662.

[16] a) R. Pummerer, E. Prell, A. Rieche, *Ber. dtsch. Chem. Ges. A/B* **1926**, *59*, 2159–2161; b) R. Pummerer, A. Rieche, *Ber. dtsch. Chem. Ges. A/B* **1926**, *59*, 2161–2175.

[17] A. Rossignon, D. Bonifazi, *Synthesis* **2019**, *51*, A–L.

[18] a) T. Kaposi, S. Joshi, T. Hoh, A. Wiengarten, K. Seufert, M. Paszkiewicz, F. Klappenberger, D. Écija, L. Đorđević, T. Marangoni, D. Bonifazi, J. V. Barth, W. Auwärter, *ACS Nano* **2016**, *10*, 7665–7674; b) L. Đorđević, T. Marangoni, M. Liu, R. De Zorzi, S. Geremia, A. Minoia, R. Lazzaroni, Y. Ishida, D. Bonifazi, *ChemPlusChem* **2019**, *84*, 1270–1278.

[19] a) B. K. Bandlish, H. J. Shine, *J. Org. Chem.* **1977**, *42*, 561–563; b) N. G. Connelly, W. E. Geiger, *Chem. Rev.* **1996**, *96*, 877–910.

[20] a) P. V. R. Schleyer, C. Maerker, A. Dransfeld, H. Jiao, N. J. R. van Eikema Hommes, *J. Am. Chem. Soc.* **1996**, *118*, 6317–6318;

b) D. Geuenich, K. Hess, F. Köhler, R. Herges, *Chem. Rev.* **2005**, *105*, 3758-3772.

[21] P. Batail, K. Boubekeur, M. Fourmigué, J.-C. P. Gabriel, *Chem. Mater.* **1998**, *10*, 3005-3015.

[22] C. Kröhnke, V. Enkelmann, G. Wegner, *Angew. Chem. Int. Ed.* **1980**, *19*, 912-919.

[23] F. Mehran, B. A. Scott, *Phys. Rev. Lett.* **1973**, *31*, 1347-1349.

[24] G. Givaja, P. Amo-Ochoa, C. J. Gómez-García, F. Zamora, *Chem. Soc. Rev.* **2012**, *41*, 115-147.

[25] T. Murata, C. Yamada, K. Furukawa, Y. Morita, *Commun. Chem.* **2018**, *1*, 47.

[26] a) E. Coronado, P. Day, *Chem. Rev.* **2004**, *104*, 5419-5448; b) P. Batail, *Chem. Rev.* **2004**, *104*, 4887-4890.

[27] a) Y. Le Gal, T. Roisnel, P. Auban-Senzier, N. Bellec, J. Íñiguez, E. Canadell, D. Lorcy, *J. Am. Chem. Soc.* **2018**, *140*, 6998-7004; b) M. A. Christensen, C. R. Parker, T. J. Sørensen, S. de Graaf, T. J. Morsing, T. Brock-Nannestad, J. Bendix, M. M. Haley, P. Rapta, A. Danilov, S. Kubatkin, O. Hammerich, M. B. Nielsen, *J. Mater. Chem. C* **2014**, *2*, 10428—10438.

[28] L. Sun, M. G. Campbell, M. Dincă, *Angew. Chem. Int. Ed.* **2016**, *55*, 3566-3579.